



THE UNIVERSITY *of* EDINBURGH

Edinburgh Research Explorer

Extraordinarily complex crystal structure with mesoscopic patterning in barium at high pressure

Citation for published version:

Loa, I, Nelmes, RJ, Lundegaard, LF & McMahon, MI 2012, 'Extraordinarily complex crystal structure with mesoscopic patterning in barium at high pressure', *Nature Materials*, vol. 11, no. 7, pp. 627-632.
<https://doi.org/10.1038/nmat3342>

Digital Object Identifier (DOI):

[10.1038/nmat3342](https://doi.org/10.1038/nmat3342)

Link:

[Link to publication record in Edinburgh Research Explorer](#)

Document Version:

Peer reviewed version

Published In:

Nature Materials

Publisher Rights Statement:

Author's Post-print: subject to Restrictions below, author can archive post-print (ie final draft post-refereeing)
Restrictions: 6 months embargo

General rights

Copyright for the publications made accessible via the Edinburgh Research Explorer is retained by the author(s) and / or other copyright owners and it is a condition of accessing these publications that users recognise and abide by the legal requirements associated with these rights.

Take down policy

The University of Edinburgh has made every reasonable effort to ensure that Edinburgh Research Explorer content complies with UK legislation. If you believe that the public display of this file breaches copyright please contact openaccess@ed.ac.uk providing details, and we will remove access to the work immediately and investigate your claim.



Extraordinarily complex crystal structure with mesoscopic patterning in barium at high pressure

I. Loa,* R. J. Nelmes, L. F. Lundegaard, and M. I. McMahon
SUPA, School of Physics and Astronomy, and Centre for Science at Extreme Conditions,
The University of Edinburgh, Mayfield Road, Edinburgh, EH9 3JZ, United Kingdom
(Dated: March 9, 2012)

Elemental barium adopts a series of high-pressure phases with such complex crystal structures that some of them have eluded structure determination for many years. Using single-crystal synchrotron x-ray diffraction and new data analysis strategies, we have now solved the most complex of these crystal structures, that of phase Ba-IVc at 19 GPa. It is a commensurate host-guest structure with 768 atoms in the basic unit, where the relative alignment of the guest-atom chains can be represented as a two-dimensional pattern with interlocking S-shaped 12-chain motifs repeating regularly in one direction and repeating with constrained disorder in the other. The existence of such patterning on the nanometre-scale points at medium-range interactions that are not fully screened by the itinerant electrons in this metal. Based on first-principles electronic structure calculations, pseudopotential theory and an analysis of the lattice periodicities and interatomic distances, we rationalise why the Ba phases with the common densely-packed crystal structures become energetically unfavourable compared to the complex-structured Ba-IVc phase, and what the role of the well-known pressure-induced s - d electronic transfer is.

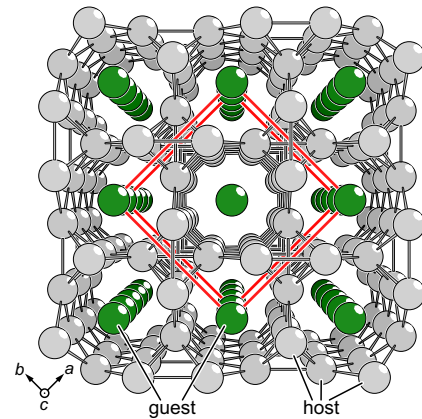


FIG. 1. Basic host-guest motif of the Ba-IV crystal structures. The red lines indicate the basic host unit cell.

At ordinary conditions of pressure and temperature, most elemental metals crystallise in simple, densely-packed crystal structures. Over the past decade, however, many elements have been discovered to adopt unexpectedly complex structures when subjected to high pressure^{1,2}. A case in point is barium which has the body-centred cubic (bcc) crystal structure at one atmosphere. Upon compression, it first transforms to hexagonal close-packed (hcp) at 5 GPa and then goes through a whole series of phases with complex structures between 12 and 45 GPa^{3,4} before returning to hcp, which is stable to at least 90 GPa⁵. The structures of all the complex phases are related and we refer to them all together as Ba-IV. The first member of this sequence, Ba-IVa, has an incommensurate host-guest crystal structure³, where some of the Ba atoms form a three-dimensional framework (the ‘host’) with open channels that accommodate the remainder of the Ba atoms in linear chains (the ‘guest’) as shown in Fig. 1. The periodicities of the host and the guest substructure are incommensurate with each other, i.e., they have a non-rational ratio. For more than a decade, additional phases have been known to exist in the Ba-IV sequence (Ba-IVb, c and d), but their structures were too complex to be solved from powder diffraction data^{3,4}.

It is of great interest to understand the fascinating crystal structures of the complex phases in Ba and numerous other elements, the reasons for their formation and the associated changes in the physical properties, such as lithium and sodium turning non-metallic at high compression^{6,7}. However, the determination of such very complex elemental structures has proven to be extremely difficult, even when single-crystal diffraction data are available. Our initial efforts to solve the Ba-IVc structure by conventional crystallographic techniques, i.e. *direct methods*⁸⁻¹⁰, did not yield conclusive results. An alternative approach, starting from a computational random search, was therefore developed for the solution of what we believe to be by far the most complex crystal structure known to exist in a pure element.

The crystal structure of Ba-IVc was studied at room temperature by synchrotron x-ray diffraction and using diamond anvil cells for high-pressure generation. The phase Ba-IVc is stable in the range 18–21 GPa, where the density is ~ 2.35 times that at zero pressure. Figure 2 shows the reciprocal-space mappings of the single-crystal diffraction data for the $(hk4)$ and $(hk\bar{4})$ layers at 19 GPa. Reflections in these layers originate from the guest substructure and form a diffraction pattern of extraordinary complexity with an exotic combination of sharp and diffuse reflections in a highly systematic arrangement. The inset in Fig. 2 highlights the weakest diffraction features – secondary diffuse reflections and extremely weak sharp reflections. Additional diffraction images are shown in the Supplementary Information. Such a combination of sharp spots and reflections that are broadened along one direction in reciprocal space is rather unusual for an elemental crystal, but related effects have been observed for inorganic compounds and protein crystals¹¹. The nature of the diffraction pattern indicates that the guest-atom structure combines long-range-ordered and disordered elements, very different from the complete chain disorder (“chain melting”) observed previously in the host-guest

* e-mail: I.Loa@ed.ac.uk

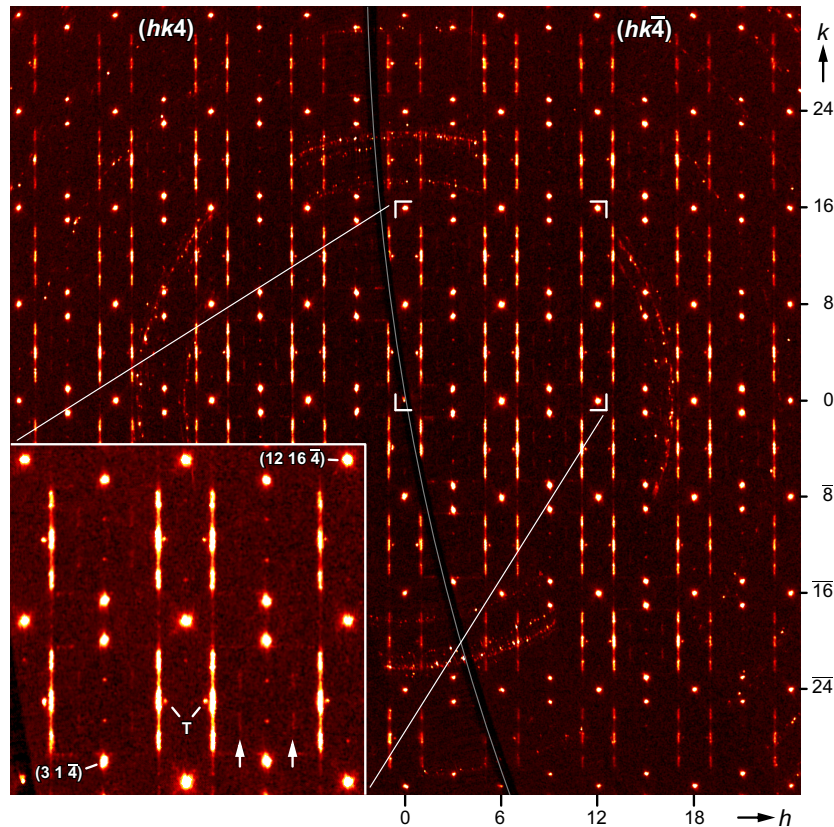


FIG. 2. Single-crystal x-ray diffraction data of Ba-IVc at 19 GPa. Reciprocal-space mappings of the $(hk4)$ and $(hk\bar{4})$ layers of guest reflections are shown in the left and the right part of the image, respectively, and separated by a dark arc marked by a central grey line. The spotty partial rings are due to diffraction from the Be seats of the diamond anvil cell, and the dark arc is a shadow at the boundary of the data accessible through the circular opening of the pressure cell. The inset shows characteristic details enlarged with an enhanced intensity scale. ‘T’ marks weak diffraction spots from a minor twin crystal, and the arrows point at lines of secondary diffuse reflections. Two of the strong and sharp reflections are indexed.

phase of rubidium^{12,13}.

An analysis of only the strongest sharp reflections confirmed that the Ba-IVc structure is derived from the basic host-guest structural motif shown in Fig. 1. Unlike in the incommensurate host-guest structures of barium at lower pressure and in other elements², the host and guest components in Ba-IVc are commensurate, and the motif has 8 host and $2\frac{2}{3}$ guest atoms in the basic Ba-IV unit cell. The full set of sharp and diffuse reflections can be indexed using a $3\sqrt{2} \times 4\sqrt{2} \times 3$ supercell of the basic host unit cell with dimensions $33.99 \times 45.46 \times 13.41 \text{ \AA}^3$. This is 72 times the volume of the basic host unit cell, and hence there are 768 atoms in the supercell of Ba-IVc!

As we will see below, the crystal structure lacks translational symmetry along one direction (along b) so that neither a crystallographic unit cell nor a space group can be assigned. On the other hand, indexing the observed sharp and diffuse reflections requires the $34 \times 45 \times 13 \text{ \AA}^3$ lattice, and this is also the size of the smallest possible unit cell of fully-ordered variants of this structure (Supplementary Information). It is therefore appropriate to discuss the Ba-IVc structure in terms of a ‘basic unit’ of that size, containing 768 atoms.

The solution of the full crystal structure proved a significant challenge. As initial efforts to solve the structure by di-

rect methods^{8–10} did not yield conclusive results, we attempted to obtain a first model of the guest substructure from a computational random search. Several thousand trial structures were generated, the guest atom positions were optimised so as to minimise the difference between calculated and measured diffraction intensities, and finally the recurring structural motifs of the best solutions were identified. On the basis of these motifs, a series of structure models was developed that included more and more structural details, which eventually explained and reproduced the experimentally observed diffraction patterns to a remarkable degree as shown in Fig. 4 and as detailed in the Supplementary Information.

Our final model of the full Ba-IVc host-guest crystal structure is illustrated in Fig. 3, with the guest substructure being of particular interest. All the chains of guest atoms take one of only two different positions along the chain direction (the c direction), which we will call the ‘up’ and the ‘down’ positions hereafter. In Fig. 3, the ‘up’ and ‘down’ chains are coloured yellow and blue, respectively, and from the relative arrangement of the two types of chains an intricate two-dimensional pattern emerges (Fig. 3c). The pattern consists of intertwined S-shaped units, each comprising 12 adjacent chains of the same type, ‘up’ or ‘down’. At first glance, the pattern in Fig. 3c looks well-ordered, but it contains both these S-shaped units

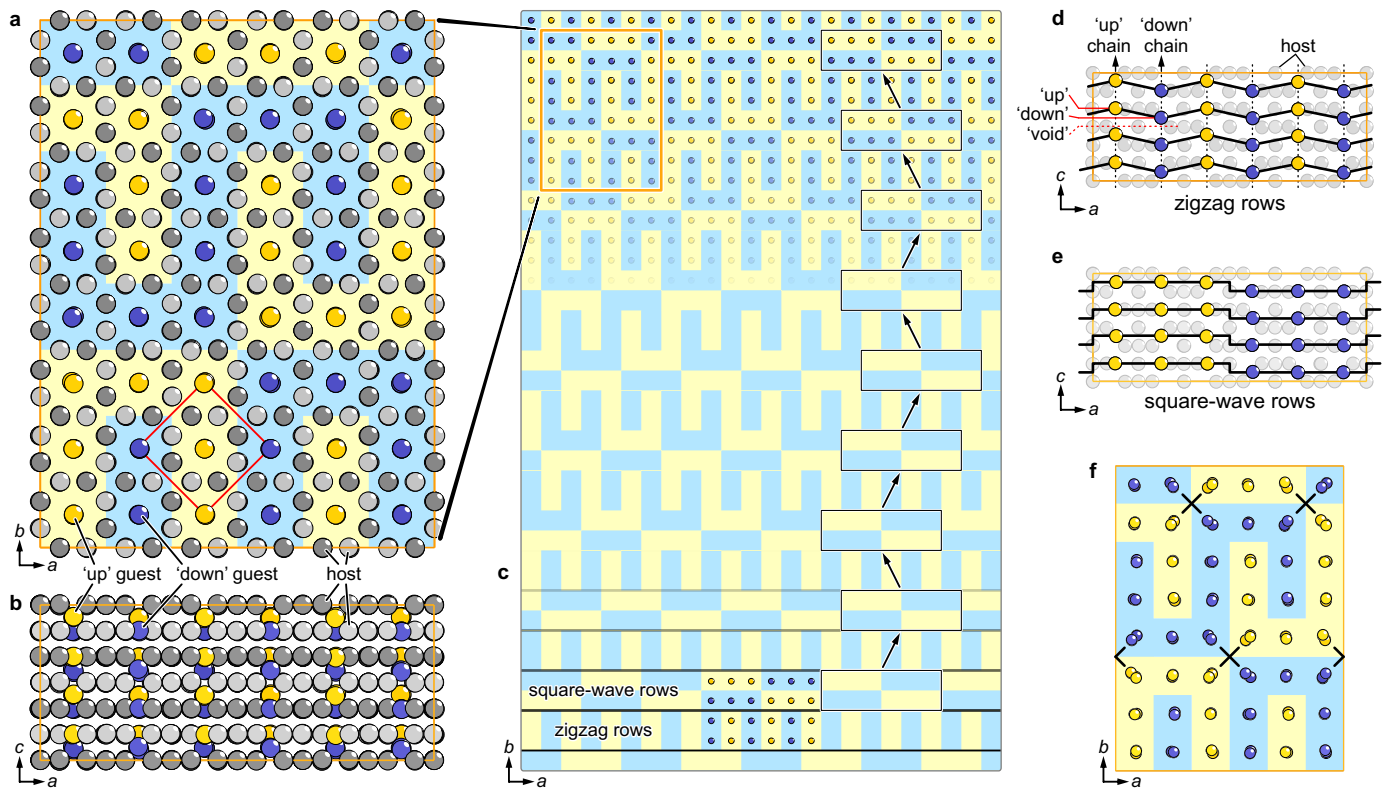


FIG. 3. Schematic view of the crystal structure of Ba-IVc. Projections of a 768-atom basic unit along the crystallographic c and b directions are shown in **a** and **b**, respectively. Host atoms in alternate layers perpendicular to c are shown dark and pale grey. Guest atoms in the ‘up’ and ‘down’ positions are coloured yellow and blue, respectively. Light blue and light yellow backgrounds highlight the pattern formed by the ‘up’ and ‘down’ guest chains. The red square in **a** indicates the basic Ba-IV unit cell. **c**, Pattern representing the ‘up’ and ‘down’ guest chains and decomposition into zigzag and square-wave rows, which are shown in **d** and **e**. **f**, Displacements of the guest atoms perpendicular to the chain direction. The refined atomic displacements are shown $5\times$ magnified. The chains at the corners of the S-shaped building blocks, marked ‘x’, show a clear zigzag displacement pattern.

and their mirror images, and the tiling includes an element of randomness. It is this tiling of relatively large building blocks with a certain degree of randomness that leads to the unusual diffraction patterns with sharp and diffuse reflections. We find it rather striking to observe such structural patterning in an elemental crystal, reminiscent in some ways of M. C. Escher’s drawings of plane-filling patterns¹⁴.

The interplay between long-range order and disorder becomes clearer when the guest pattern is decomposed into *zigzag rows*, where the neighbouring guest chains are alternatingly in the ‘up’ and the ‘down’ position as one proceeds along the a direction, and *square-wave rows*, where three guest atoms in the ‘up’ position are followed by three atoms in the ‘down’ position (Fig. 3c–e). Both the zigzag and the square-wave rows occur in pairs. The two rows in each pair are in-phase for the zigzag pairs and anti-phase for the square-wave pairs. These two types of double-rows along the a direction are then stacked alternately along the b direction with two constraints on their relative alignment. (i) Any three consecutive ‘up’ chains in a square-wave row are always next to an ‘up/down/up’ set of chains in the adjacent zigzag row. (ii) In moving from one square-wave double row to the next along the b direction, only displacements of exactly one step ($a/6$) along the positive or negative a di-

rection occur (left or right in Fig. 3c), and no others. These shifts left and right are random with equal probability. A consequence of these constraints is that the subset of zigzag rows is long-range-ordered while the sequence of square-wave rows is not. The latter is a “constrained-random” sequence which represents a random walk in one dimension (Supplementary Information). Among the 63 different stacking sequences produced by allowing combinations of all possible shifts (zero, $a/6$, $2a/6$ or $3a/6$, left or right), the sequence described above is the only one that reproduces the experimentally observed diffraction patterns (Fig. S3 in the Supplementary Information). Apart from small local distortions in response to the randomness in the guest substructure, the host substructure is long-range ordered. The Ba-IVc crystal structure thus combines long-range-ordered and disordered elements, and the disorder occurs on the level of relatively large units.

An idealised variant of the Ba-IVc structure, where all the guest atom chains are strictly linear, located at the centres of the host channels and with equally-spaced atoms, reproduces most of the characteristic features of the x-ray diffraction patterns. But there are reproducible features not accounted for, such as the secondary diffuse reflections in the $(hk\bar{4})$ layer (inset in Fig. 2) and all the weak diffraction spots observed in layers

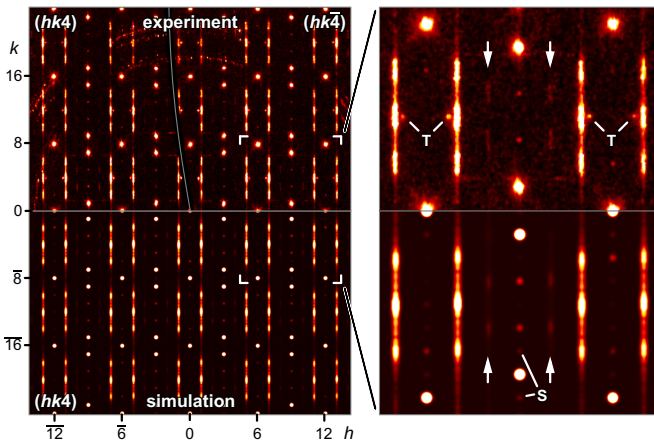


FIG. 4. Comparison of the experimental diffraction data mapped onto the $(hk4)$ and $(hk\bar{4})$ reciprocal space planes (top half) and the simulated pattern for the final Ba-IVc structural model (bottom half). The magnified part highlights the weakest features with an enhanced intensity scale, and the faint horizontal lines in the top part are due to diffraction from a minor twin crystal, which causes also the reflections marked ‘T’. The arrows point at lines of secondary diffuse reflections. ‘S’ marks weak satellite reflections in the simulation that are not observed experimentally. They arise because the final model of the *host* structure was constrained to be completely ordered — it does not include local distortions in response to the randomness in the guest substructure (Supplementary Information). The fine structure of the experimental diffuse reflections is an artefact of the mapping process and that of the simulated diffuse reflections originates from the finite approximation of the constrained-random stacking sequence.

such as $(hk5)$ and $(hk7)$, and these are due to small displacements of host and guest atoms away from the idealised positions. Because of the many degrees of freedom combined with the randomness in the Ba-IVc structure, a complete determination of the locally relaxed structure is hardly feasible from diffraction data alone. We have performed a constrained refinement of the atomic positions, which was still a formidable optimisation task with a total of 2016 refinable atomic coordinates (Supplementary Information), but with the single-crystal data set comprising nearly 14,000 measured intensities (independent reflections, including near-zero intensities), it is a well-defined problem.

Small atomic displacements of, on average, 1% of the nearest-neighbour distances are sufficient to reproduce even the weakest features of the experimental diffraction data. Figure 4 shows a direct comparison of the $(hk4)$ mapping of the experimental data and a simulation based on our final model of the Ba-IVc crystal structure with refined atomic coordinates and using a $30\times$ supercell (along b) of the Ba-IVc basic unit, comprising a total of 23,040 atoms, to approximate the randomness in the structure. To a remarkable degree, the simulation reproduces all the observed features, the combination of sharp and diffuse reflections and even the secondary diffuse reflections. The diffraction patterns for other reciprocal-space layers are reproduced to the same degree. The refinement also uncovered further structural details, in particular that the guest atom chains at the corners of the S-shaped units have a zigzag mod-

ulation with displacements perpendicular to the chain direction (Fig. 3f).

The crystal structure of Ba-IVc takes the structural complexity uncovered in metallic elements to a new extreme, and shows in a dramatic way what very different states can emerge at higher densities. An important new aspect is the emergence of a structural patterning on a length scale much larger (>20 Å) than the nearest-neighbour distances of ~ 3.2 Å. It highlights the importance of medium-range interactions that one might have expected to be insignificant because of the screening by the itinerant electrons in a metal.

To characterise the electronic properties of Ba-IVc, we performed first-principles electronic structure calculations in the framework of full-potential density functional theory (DFT) for two simplified approximants of Ba-IVc (Supplementary Information). The complex chain pattern was approximated by (i) a checkerboard pattern, where the chains are in the ‘up’ and the ‘down’ position alternatingly along both the a and the b direction, and by (ii) a stripe pattern, where the chains alternate between the ‘up’ and ‘down’ positions only along one direction. The calculations yield the following picture: (i) The approximants have “normal” metallic densities of states without a pseudogap near the Fermi level. The Ba-IVc structure thus appears not to be stabilised by Fermi-surface Brillouin-zone interactions as proposed previously for several alkali and alkaline earth high-pressure phases^{15,16}. (ii) There is no significant difference in electronic structure between the host and the guest atoms – at variance with suggestions for the lower-pressure phase Ba-IVa, which has been considered an intermetallic compound in which both components are the same element¹⁷. (iii) As discussed before^{18,19}, the valence state of Ba changes under pressure with electrons being transferred from s - and p - to d -type states (“ s - d transfer”). The peak occupation of d states occurs in the stability range of Ba-IV and coincides with the onset of the d - f transfer that occurs under further compression. A decomposition of the conduction band states of the Ba-IVc approximants yields 80% d character, 10% p , 5% s and 5% f at 19 GPa. (iv) The calculated charge density distributions of the approximants have no maxima at interstitial positions, in contrast to the situation in the alkali metals at high density^{20–26}, where the interpretation of the interstitial maxima in terms of an electride-type behaviour has recently attracted renewed interest. Particularly noteworthy is the difference between Ba and Cs, which are neighbours in the periodic table and which are both essentially d transition metals at ~ 20 GPa, with only Cs having interstitial charge-density maxima²². Altogether, Ba-IVc appears to be a rather normal metal, except for its unusual electronic configuration close to $[\text{Xe}]5d^2$.

The stability of complex elemental high-pressure phases has been reproduced in DFT calculations (see, for example, Refs. 17, 27, and 28), and their existence in alkali and alkaline earth metals has repeatedly been attributed to electronic transfers (s to p or d). However, a physical picture of how this valence change leads to the complex phases appears to be lacking. Clearly, the experimentally observed complex structures must have a lower free energy than the simpler, densely-packed alternatives, but can we rationalise why this is so and what the significance of the s - d transfer in Ba is?

The crystal structures of most metals are determined by the competition between the two dominant contributions to the total energy: the electrostatic (Madelung) term, which favours densely-packed crystal structures, and the electronic band structure term, which favours open structures²⁹. We have extended the above *ab initio* calculations to calculate the total energies of bcc, fcc and hcp Ba, all at the experimental density of Ba-IVc at 19 GPa. Among these ideal densely-packed structures, we found hcp ($c/a = 1.63$) to have the lowest total energy. The total energy of hcp can be lowered further, by a considerable 23 meV/atom, by reducing the c/a ratio to 1.46 (cf. Refs. 5 and 30).

This reduced c/a ratio represents an appreciable departure from close-packing both in terms of the interatomic distances and in terms of the Madelung energy: the difference in electrostatic energy between the distorted hcp and ideal hcp is 17× larger than the difference between ideal hcp and bcc. The finding that the distorted hcp structure nonetheless has the lowest total energy among the simple structures illustrates how the cost in electrostatic energy can be more than compensated by a gain in band-structure energy. It also highlights how energetically unfavourable the ideal densely-packed structures are in Ba at around 20 GPa, and this opens the way for more complex crystal structures to become energetically advantageous – with Ba-IVc being an extreme case.

In the 1960s, Heine and Weaire developed a physical picture of how the structural stability of elemental metals is related to the shape of their atomic pseudopotentials^{31–33}. The key point is that a crystal structure tends to be energetically unfavourable if one or more reciprocal lattice points \mathbf{g} (or Bragg reflections) with large structure factors $S(\mathbf{g})$ are close in magnitude to the position of the first zero of the pseudopotential $v(q)$ – because it reduces the bandstructure contribution to the binding energy.

The Heine-Weaire approach provides valuable insight into why the simple structures of Ba are destabilised under pressure. At 20 GPa, the Ba d valence states are dominant with a contribution of ~80%, and, as explained in detail in the Supplementary Information, the bcc, fcc and hcp structures suffer energetically from having strong reflections close to the first zero of the d -channel of the Ba pseudopotential, q_0^d . Figure 5 illustrates how lowering the c/a ratio of the hcp structure to 1.46 alleviates this unfavourable situation: it moves two quite strong reflections away from the zero of the pseudopotential, q_0^d , and consequently increases the bandstructure contribution to the binding energy. This relatively simple picture rationalises why the heavily-distorted hcp structure is the most stable among the densely-packed structures. It also shows that, and why, the energetics depend crucially on the occupation of the d orbitals (as pointed out previously by Zeng *et al.*¹⁹) and reveals thereby the significance of the pressure-induced s – d transfer.

The application of pressure has thus two important effects: it increases the occupation of the Ba d orbitals, which rises to a maximum at about 20 GPa, and it changes the lattice periodicities of the densely-packed structures in relation to the atomic pseudopotential. As a result, the densely-packed structures become unfavourable in the pressure range around 20 GPa, and the Ba-IV phases are stabilised. Due to the large unit cell, the Ba-IVc phase has a much larger number of contributions to the

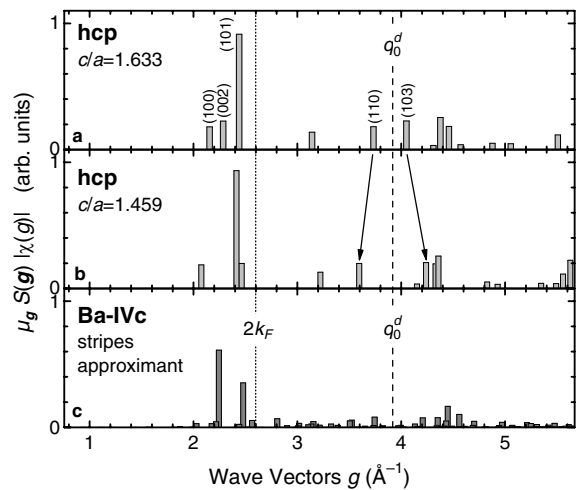


FIG. 5. Structural weights, $\mu_g S(\mathbf{g})|\chi(\mathbf{g})|$, for hcp Ba and the Ba-IVc stripes approximant at 19 GPa. μ_g is the multiplicity of reciprocal-lattice point \mathbf{g} and $\chi(\mathbf{g})$ the Lindhard dielectric function. The positions of the first zero of the d -channel of the Ba pseudopotential, q_0^d , and twice the Fermi wave vector, $2k_F$, are indicated by vertical lines.

band structure energy than the simple structures, and they are more spread out in wave vector (Fig. 5). The Ba-IVc structure, like distorted hcp, benefits from not having strong reflections close to q_0^d , and the sum of its structural weights is indistinguishable from that of distorted hcp. To explain why Ba-IVc is the energetically favourable of the two phases is clearly beyond the scope of the semi-quantitative Heine-Weaire picture, which focuses on the relation between the atomic pseudopotential and the lattice periodicities, but neglects other potentially important aspects of the energetics. However, the stability of Ba-IVc is reproduced in our DFT calculations: the checkerboard and stripe approximants of Ba-IVc are 1 and 7 meV/atom, respectively, lower in energy than the distorted hcp ($c/a = 1.46$) structure. These results also indicate that there are significant energetic differences between Ba-IVc-type structures with different chain patterns – and there are countless possible patterns to choose from.

Important insight into what stabilises Ba-IV comes from a comparison of the distributions of the interatomic distances of the various structure candidates (Supplementary Information). At 19 GPa, each atom in Ba-IVc (and both approximants) has on average 6.5 neighbours at a distance of ~4.4 Å. This is the distance where the minimum of the pair interaction potential is located during the s – d transfer for a 80% d + 20% s configuration¹⁹. Having atoms at the optimal, “strongest-binding” distance sets the Ba-IVc structure (in fact, all the Ba-IV structures) apart from the simple structures, and we consider this to be the key ingredient for the stability of the Ba-IV phases.

In essence, the occupation of Ba d valence states increases under compression and peaks at around 20 GPa. In the same pressure range, the simple structures happen to have strong Bragg reflections with wavevectors close in magnitude to the first zero of the d channel of the Ba pseudopotential. This re-

duces the band structure contribution to the binding energy and renders the simple crystal structures energetically unfavourable. The Ba-IVc structure avoids this and also benefits energetically from having atoms at the optimal interatomic distance corresponding to the minimum of the pair interaction potential, while its departure from close-packing is moderate in terms of the Madelung energy (Supplementary Information). Ba-IVc thus appears to be stabilised by the fundamental contributions to the binding energy, and effects such as Fermi-surface Brillouin-zone interaction discussed previously^{15,16} play only a minor role, if any.

It would be desirable to understand how the complex Ba-IV crystal structures affect the physical properties of barium, but experimental studies have remained scarce. Noteworthy is the observation that the electrical resistivity increases markedly at the hcp→Ba-IV transition³⁴ and that the superconducting transition temperature peaks at around 20 GPa with $T_c = 5$ K³⁵. New measurements would now be well worthwhile and, in view of the anisotropy of the structures, measurements on single-crystal samples would be particularly interesting, though difficult to perform.

Looking beyond Ba and its extraordinary crystal structures, we should point out that pressure-induced s - d and s - p electronic transfers are a recurring theme for all alkali and alkaline earth elements under compression. It appears likely that a destabilisation of the close-packed crystal structures takes place not only in Ba as discussed here, but also in other elements. It thus seems worthwhile to use the Heine-Weaire approach as a starting point of future studies on the complex crystal structures^{1,2} of other elements at high pressure.

Extremely complex crystal structures exist also in seemingly simple intermetallic compounds such as the Samson phases NaCd₂ and β -Mg₂Al₃, both with over 1000 atoms per cubic unit cell^{36,37}, and in ternary Al-Cu-Ta phases with up to 23,000 atoms per cubic unit cell³⁸. All of these structures can be described in terms of hierarchies of clusters, and they are therefore very different from the host-guest structures in barium and other elements. On the other hand, the Samson phases do also have an element of randomness or disorder. With the constrained-random stacking sequence of Ba-IVc in mind, one may wonder whether the disorder in NaCd₂ and β -Mg₂Al₃ may be of similar origin. Like for the elemental systems, the understanding of the origin of the complexity in intermetallic compounds is still fraught with uncertainties^{39,40}. Considering the similarities and differences between these very different systems in future research may thus be beneficial for the understanding of each of them.

METHODS AND MATERIALS

Sample preparation Individual pieces of barium with typical dimensions of 30–100 μ m were cut off a dendritic ingot of high-purity, distilled barium with a stated purity of 99.99%

(Sigma-Aldrich) and loaded into Merrill-Bassett-type diamond anvil cells (DACs). Mineral oil was used as a pressure transmitting medium and to avoid bridging of the samples between the diamond anvils. The sample loading was performed under inert argon atmosphere. A small ruby sphere was enclosed with the sample in the DAC for pressure determination^{41,42}. Most of the samples were then pressurised to ~ 15 GPa at room temperature and subsequently annealed at $\sim 200^\circ\text{C}$ for 12 hours or longer. After slowly cooling to room temperature, single-crystals of the phase Ba-IVa were obtained in several cases. These single-crystal samples were then pressurised to 18–21 GPa to obtain single-crystal samples of the phase Ba-IVc.

X-ray diffraction Single-crystal x-ray diffraction experiments were performed on beamline ID27 at the European Synchrotron Radiation Facility (ESRF), Grenoble, France. The x-ray beam of wavelength 0.25 Å was focussed onto the sample in the DAC with an x-ray spot size of less than 5 μ m (full width at half maximum). Diffraction images were collected with a Marresearch MarCCD detector placed at a distance of ~ 250 mm from the sample. The diffraction data were collected in a sequence of contiguous 0.2–0.3° oscillations ($\Delta\omega$) over a total scan range of 60–80° around the vertical axis. Typically, short exposure times of 0.1–0.2 s per frame were used to avoid saturation of the strongest peaks, and additional data sets were collected with exposure times of ~ 2 s to improve the signal/noise ratio for the very weak reflections. Further diffraction experiments were conducted on beamline 9.5HPT at the former Synchrotron Radiation Source (SRS), Daresbury Laboratory using an x-ray wavelength of 0.44 Å and a Mar345 image plate detector.

Data analysis The MarCCD image files were converted to the Bruker frame format for analysis using the Bruker SMART, SAINT and SADABS programs⁴³. For the data set that was used for the full structure refinement, reflection intensities were integrated using SAINT, and reflections with measured positions that deviated from the expected positions by more than 0.5 pixels or $\Delta\omega/2$ were filtered out. The intensities were rescaled using the SADABS software to correct for changes in scattering volume during the rotation of the irregular-shaped Ba sample. The CrysAlis RED software⁴⁴ was used to produce reciprocal-space mappings (reconstructions of precession photographs) of the experimental diffraction data for selected planes in reciprocal space. For the various steps of the Ba-IVc crystal structure determination and analysis, several computer programs were developed using the Python programming language⁴⁵ and the OpenOpt package⁴⁶ for numerical optimisation.

DFT calculations First-principles electronic structure calculation were performed in the framework of density functional theory as implemented in the full-potential, augmented plane-wave WIEN2k code⁴⁷ and using the generalised gradient approximation (GGA)⁴⁸. The Ba 4*d*, 5*s*, 5*p*, 5*d*, 6*s* states were treated as valence states, and a Brillouin zone integration mesh with a spacing of approximately $2\pi \times 0.015$ Å⁻¹ was used for all structures (e.g., a $22 \times 22 \times 22$ grid for bcc). Other parameters were $R_{\text{MT}} \times K_{\text{max}} = 9.0$, $R_{\text{MT}} = 2.5$ a.u., $l_{\text{max}} = 10$, $G_{\text{max}} = 16$.

- ¹ Schwarz, U. Metallic High-Pressure Modifications of Main Group Elements. *Z. Kristallogr.* **219**, 376–390 (2004).
- ² McMahon, M. I. & Nemes, R. J. High-pressure structures and phase transformations in elemental metals. *Chem. Soc. Rev.* **35**, 943–963 (2006).
- ³ Nemes, R., Allan, D., McMahon, M. & Belmonte, S. Self-Hosting Incommensurate Structure of Barium IV. *Phys. Rev. Lett.* **83**, 4081–4084 (1999).
- ⁴ Nemes, R. J., McMahon, M. I., Allan, D., Belmonte, S. & Bovorn-ratanaraks, T. Incommensurate Structures of Ba-IV and Sr-V. In *Science and Technology of High Pressure, Proceedings of AIRAPT-17* (eds Manghnani, M., Nellis, W. & Nicol, M.), 475–478 (Universities Press, Hyderabad, India, 2000).
- ⁵ Takemura, K. High-pressure structural study of barium to 90 GPa. *Phys. Rev. B* **50**, 16238–16246 (1994).
- ⁶ Matsuoka, T. & Shimizu, K. Direct observation of a pressure-induced metal-to-semiconductor transition in lithium. *Nature* **458**, 186–189 (2009).
- ⁷ Ma, Y. *et al.* Transparent dense sodium. *Nature* **458**, 182–185 (2009).
- ⁸ Altomare, A. *et al.* SIR92 – a program for automatic solution of crystal structures by direct methods. *J. Appl. Cryst.* **27**, 435 (1994).
- ⁹ Sheldrick, G. M. A short history of SHELX. *Acta Cryst. A* **64**, 112–122 (2008).
- ¹⁰ Farrugia, L. WinGX suite for small-molecule single-crystal crystallography. *J. Appl. Cryst.* **32**, 837–838 (1999).
- ¹¹ Wang, J., Kamtekar, S., Berman, A. J. & Steitz, T. A. Correction of X-ray intensities from single crystals containing lattice-translocation defects. *Acta Cryst. D* **61**, 67–74 (2005).
- ¹² McMahon, M. I. & Nemes, R. J. Chain “Melting” in the Composite Rb-IV Structure. *Phys. Rev. Lett.* **93**, 055501 (2004).
- ¹³ Falconi, S. *et al.* X-ray diffraction study of diffuse scattering in incommensurate rubidium-IV. *Phys. Rev. B* **73**, 214102 (2006).
- ¹⁴ http://euler.slu.edu/escher/index.php/Regular_Division_of_the_Plane_Drawings.
- ¹⁵ Ackland, G. J. & Macleod, I. R. Origin of the complex crystal structures of elements at intermediate pressure. *New J. Phys.* **6**, 138 (2004).
- ¹⁶ Degtyareva, V. F. Simple metals at high pressures: the Fermi sphere – Brillouin zone interaction model. *Physics–Uspekhi* **49**, 369 (2006).
- ¹⁷ Reed, S. K. & Ackland, G. J. Theoretical and Computational Study of High-Pressure Structures in Barium. *Phys. Rev. Lett.* **84**, 5580–5583 (2000).
- ¹⁸ Moriarty, J. A. First-principles phonon spectrum in bcc Ba: Three-ion forces and transition-metal behavior. *Phys. Rev. B* **34**, 6738–6745 (1986).
- ¹⁹ Zeng, W.-S., Heine, V. & Jepsen, O. The structure of barium in the hexagonal close-packed phase under high pressure. *J. Phys.: Condens. Matter* **9**, 3489 (1997).
- ²⁰ Neaton, J. B. & Ashcroft, N. W. Pairing in dense lithium. *Nature* **400**, 141–144 (1999).
- ²¹ Hanfland, M., Syassen, K., Christensen, N. E. & Novikov, D. L. New high-pressure phases of lithium. *Nature* **408**, 174 (2000).
- ²² Schwarz, U., Jepsen, O. & Syassen, K. Electronic structure and bonding in the *Cmca* phases of Si and Cs. *Solid State Commun.* **113**, 643–648 (2000).
- ²³ Rousseau, B. & Ashcroft, N. W. Interstitial Electronic Localization. *Phys. Rev. Lett.* **101**, 046407 (2008).
- ²⁴ Pickard, C. J. & Needs, R. J. Dense Low-Coordination Phases of Lithium. *Phys. Rev. Lett.* **102**, 146401 (2009).
- ²⁵ Marqués, M. *et al.* Potassium under Pressure: A Pseudobinary Ionic Compound. *Phys. Rev. Lett.* **103**, 115501 (2009).
- ²⁶ Rousseau, B., Xie, Y., Ma, Y. & Bergara, A. Exotic high pressure behavior of light alkali metals, lithium and sodium. *Eur. Phys. J. B* **81**, 1–14 (2011).
- ²⁷ Schwarz, U. *et al.* Structure and stability of the modulated phase Sb-II. *Phys. Rev. B* **67**, 214101 (2003).
- ²⁸ Arapan, S., Skorodumova, N. V. & Ahuja, R. Determination of the Structural Parameters of an Incommensurate Phase from First Principles: The Case of Sc-II. *Phys. Rev. Lett.* **102**, 085701 (2009).
- ²⁹ Skriver, H. Crystal structure from one-electron theory. *Phys. Rev. B* **31**, 1909 (1985).
- ³⁰ Jona, F. & Marcus, P. M. Structure of barium in three phases under pressure. *Europhys. Lett.* **74**, 83 (2006).
- ³¹ Heine, V. & Weaire, D. Pseudopotential theory of cohesion and structure. *Sol. State Phys.* **24**, 249–463 (1970).
- ³² Animalu, A. O. E. Electronic Theory of Phase Transitions in Ca, Sr, and Ba under Pressure. *Phys. Rev.* **161**, 445–455 (1967).
- ³³ Hafner, J. & Heine, V. The crystal structures of the elements: pseudopotential theory revisited. *J. Phys. F: Metal Phys.* **13**, 2479 (1983).
- ³⁴ Wittig, J. & Matthias, B. T. Superconductivity of Barium Under Pressure. *Phys. Rev. Lett.* **22**, 634–636 (1969).
- ³⁵ Dunn, K. J. & Bundy, F. P. Pressure-induced superconductivity in strontium and barium. *Phys. Rev. B* **25**, 194–197 (1982). And references therein.
- ³⁶ Samson, S. Crystal Structure of NaCd₂. *Nature* **195**, 259–262 (1962).
- ³⁷ Samson, S. The crystal structure of the phase β -Mg₂Al₃. *Acta Cryst.* **19**, 401–413 (1965).
- ³⁸ Weber, T. *et al.* Large, larger, largest – a family of cluster-based tantalum copper aluminides with giant unit cells. I. Structure solution and refinement. *Acta Cryst. B* **65**, 308–317 (2009).
- ³⁹ Steurer, W. *et al.* The Samson phase, β -Mg₂Al₃, revisited. *Z. Kristallogr.* **222**, 259–288 (2007).
- ⁴⁰ Fredrickson, D., Lee, S. & Hoffmann, R. Interpenetrating Polar and Nonpolar Sublattices in Intermetallics: The NaCd₂ Structure. *Angew. Chem. Int. Ed.* **46**, 1958–1976 (2007).
- ⁴¹ Piermarini, G. J., Block, S., Barnett, J. D. & Forman, R. A. Calibration of the pressure dependence of the *R*₁ ruby fluorescence line to 195 kbar. *J. Appl. Phys.* **46**, 2774–2780 (1975).
- ⁴² Mao, H. K., Xu, J. & Bell, P. M. Calibration of the Ruby Pressure Gauge to 800 kbar Under Quasi-Hydrostatic Conditions. *J. Geophys. Res.* **91**, 4673 (1986).
- ⁴³ Bruker AXS software suite, 1997.
- ⁴⁴ Computer program CrysAlis RED (version 1.171.33) by Oxford Diffraction (now Agilent Technologies).
- ⁴⁵ Python programming language, <http://www.python.org>.
- ⁴⁶ OPENOPT numerical optimization package, <http://www.openopt.org>.
- ⁴⁷ Blaha, P., Schwarz, K., Madsen, G. K. H., Kvasnicka, D. & Luitz, J. WIEN2K, An Augmented Plane Wave + Local Orbitals Program for Calculating Crystal Properties (K. Schwarz, Techn. Universität Wien, Austria, 2001).
- ⁴⁸ Perdew, J. P., Burke, K. & Ernzerhof, M. Generalized Gradient Approximation Made Simple. *Phys. Rev. Lett.* **77**, 3865 (1996).

ACKNOWLEDGEMENTS

We thank W. Crichton, M. Mezouar and A. Lennie for their help with the experiments and acknowledge helpful discussions with U. Schwarz, S. Scandolo and K. Syassen. This work was supported by research grants and a fellowship (I.L.) from the UK Engineering and Physical Sciences Research Council, and

facilities were made available by ESRF and SRS. The single-crystal x-ray diffraction experiments were performed as part of the ESRF Long Term Project HS-3090 on single crystal diffraction at extreme conditions. This work also used resources provided by the Edinburgh Compute and Data Facility (ECDF, www.ecdf.ed.ac.uk); the ECDF is partially supported by the eDIKT initiative (www.edikt.org.uk).